LETTER

doi:10.1038/nature25737

Fast quantum logic gates with trapped-ion qubits

V. M. Schäfer[1], C. J. Ballance[1], K. Thirumalai[1], L. J. Stephenson[1], T. G. Ballance[1], A. M. Steane[1] & D. M. Lucas[1]

Quantum bits (qubits) based on individual trapped atomic ions are a promising technology for building a quantum computer[1]. The elementary operations necessary to do so have been achieved with the required precision for some error-correction schemes[2–4]. However, the essential two-qubit logic gate that is used to generate quantum entanglement has hitherto always been performed in an adiabatic regime (in which the gate is slow compared with the characteristic motional frequencies of the ions in the trap[3–7]), resulting in logic speeds of the order of 10 kilohertz. There have been numerous proposals of methods for performing gates faster than this natural 'speed limit' of the trap[8–12]. Here we implement one such method[11], which uses amplitude-shaped laser pulses to drive the motion of the ions along trajectories designed so that the gate operation is insensitive to the optical phase of the pulses. This enables fast (megahertz-rate) quantum logic that is robust to fluctuations in the optical phase, which would otherwise be an important source of experimental error. We demonstrate entanglement generation for gate times as short as 480 nanoseconds—less than a single oscillation period of an ion in the trap and eight orders of magnitude shorter than the memory coherence time measured in similar calcium-43 hyperfine qubits. The power of the method is most evident at intermediate timescales, at which it yields a gate error more than ten times lower than can be attained using conventional techniques; for example, we achieve a 1.6-microsecond-duration gate with a fidelity of 99.8 per cent. Faster and higher-fidelity gates are possible at the cost of greater laser intensity. The method requires only a single amplitude-shaped pulse and one pair of beams derived from a continuous-wave laser. It offers the prospect of combining the unrivalled coherence properties[2,13], operation fidelities[2–4] and optical connectivity[14] of trapped-ion qubits with the submicrosecond logic speeds that are usually associated with solid-state devices[15,16].

Deterministic entanglement of multiple qubits—an essential prerequisite for general quantum information processing—was first achieved nearly twenty years ago using laser manipulation of qubits stored in the hyperfine ground states of trapped atomic ions[5]. Since then, progress in trapped-ion techniques, the development of more robust methods and an improved understanding of error sources have yielded a steady improvement in the precision of the fundamental two-qubit quantum logic gate, with the gate error ε_g decreasing by a factor of approximately two every two years, reaching $\varepsilon_g \approx 0.1\%$ in recent experiments[3,4]. In addition, all elementary single-qubit operations have been demonstrated with errors of less than 0.1% (refs 2–4). These error levels are already an order of magnitude below the threshold required for fault-tolerant quantum error-correction schemes[17]. By contrast, the two-qubit gate speed has remained fairly constant since the first demonstrations; the gates with the lowest reported errors had durations of 30 μs (ref. 4) and 100 μs (ref. 3). For qubits based on solid-state platforms, the interactions are much stronger, enabling much faster two-qubit operations (typically about 50 ns for superconducting circuits[15]; 480 ns for a recently demonstrated gate in silicon-based qubits[16]), but also leading to much shorter qubit coherence times (T_2^*; typically about 100 μs compared with about 1 min for atomic systems). Substantial progress has also been made in demonstrating simple algorithms and quantum simulations, which involve around 10 qubits, and in developing technologies that are amenable to scaling to larger numbers of qubits[18,19].

In previous trapped-ion experiments, the speed of the two-qubit gate operation has been limited by the use of methods that operate in an adiabatic regime with respect to the secular motional frequencies of the ions. Because these motional frequencies are typically about 1 MHz, gate durations are generally much longer than 1 μs, and attempts to increase the gate speed have resulted in larger gate errors; for example, $\varepsilon_g = 3\%$ was observed for the shortest reported gate time of $t_g = 5.3\,\mu s$ (ref. 3). (The minimum gate time given in ref. 3 (3.8 μs) is the full-width at half-maximum of the laser pulse, but for fair comparison with the gates reported here we quote the total gate time from the start of the rising edge to the end of the falling edge.) With recent progress in techniques for faster ground-state laser cooling[20], ion shuttling[21,22] and qubit readout[23], current two-qubit gate speeds threaten to be the limiting factor in the clock speed of a trapped-ion processor based on a quantum charge-coupled device (CCD) architecture[1,24], especially given that error-correction circuits typically contain more gates than

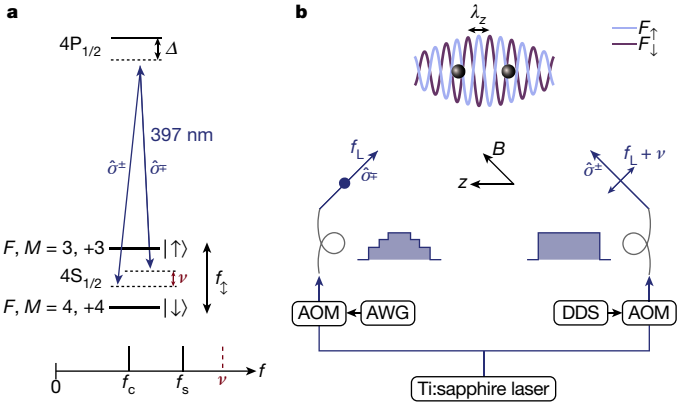

Figure 1 | Qubit states and Raman beam geometry. a, Qubits are stored in the $^{43}Ca^+$ hyperfine states $|\downarrow\rangle = 4S_{1/2}^{4,+4}$ and $|\uparrow\rangle = 4S_{1/2}^{3,+3}$, with separation $f_\updownarrow = 2.87$ GHz. The axial motional frequencies of the ion are $f_c = 1.92$ MHz and $f_s = 3.33$ MHz. The Raman beams (wavelength, 397 nm) have a mean detuning of $\Delta = -200$ GHz and a frequency difference of $\nu = 3.43 f_c$ for the fastest gate; for the highest-fidelity gates, $\Delta = -800$ GHz and $f_c < \nu < f_s$. **b**, The Raman beams of frequency f_L are derived from a single Ti:sapphire laser. One Raman beam propagates parallel to the quantization axis, set by a magnetic field $B \approx 14.6$ mT. The beams are perpendicular, such that their difference $\boldsymbol{k}$ vector is parallel to the z axis of the trap, and have waists of approximately 35 μm at the ions, powers of up to 200 mW and orthogonal linear polarizations $\hat{\sigma}^{\pm}$ and $\hat{\sigma}^{\mp}$. Their interference creates a polarization 'travelling standing wave' (period, $\lambda_z \approx 397\ \text{nm}/\sqrt{2}$) that induces a spin-dependent force ($F_\downarrow$ or $F_\uparrow$) on the ions. High-bandwidth acousto-optic modulators (AOMs) shape the laser pulses on timescales of about 10 ns; we use a constant-amplitude pulse for one beam (right) and an amplitude-shaped pulse for the other beam (left). The AOMs are driven by an arbitrary-waveform generator (AWG) and a direct digital synthesis (DDS) source.

[1]Department of Physics, University of Oxford, Clarendon Laboratory, Parks Road, Oxford OX1 3PU, UK.

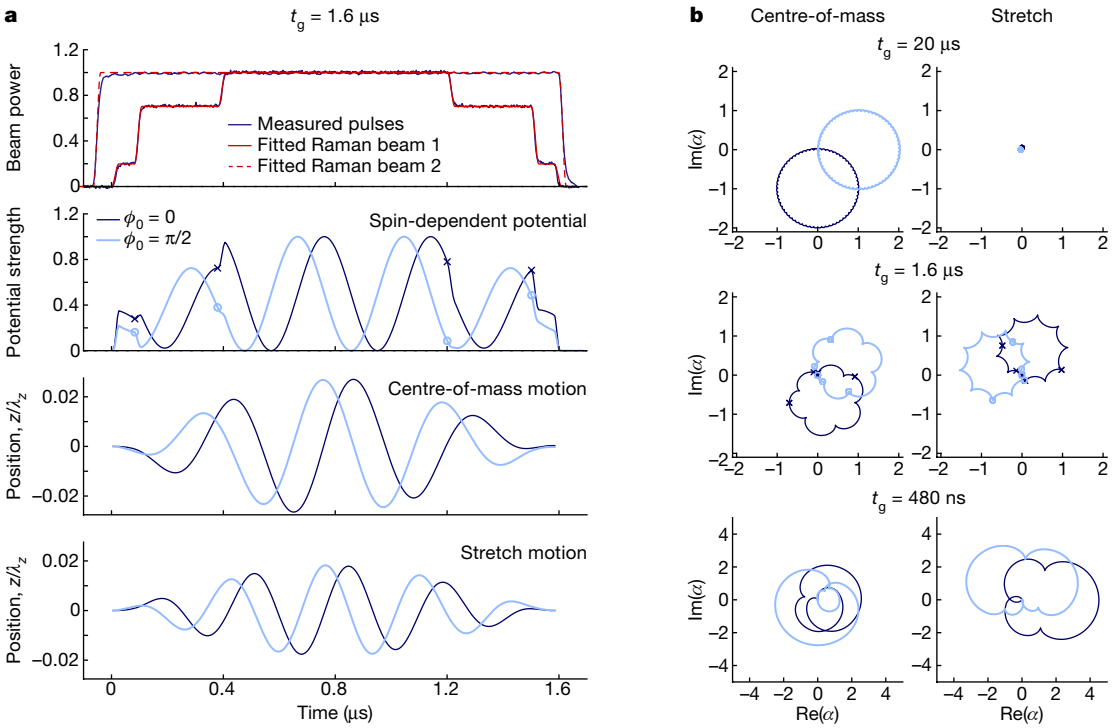

Figure 2 | Optical beat notes and motional trajectories of the ions for two initial optical phases ($\phi_0 = 0$ and $\phi_0 = \pi/2$). a, For the 1.6-μs-duration gate, the plots show: the Raman laser pulses (top); their calculated optical beat note, which gives rise to the spin- and position-dependent potential (and hence force) that the ions experience; the centre-of-mass displacement of the ions; and their stretch-mode displacement (bottom). The beat frequency is $\nu = 2.63\,\mathrm{MHz} \approx 1.37 f_c$. The force and motions clearly depend on ϕ_0; however, the shape of the pulse is designed so that, for all ϕ_0, both trajectories return to zero displacement at $t = t_g$. **b**, Phase-space trajectories for gates in three regimes (where α is the displacement in the rotating frame). For a conventional adiabatic gate ($t_g = 20\,\mu s$; top), $\nu \approx 1.03 f_c$ and the stretch mode is barely excited; ϕ_0 affects the orientation of the (nearly circular) trajectory, but not its shape or area. For $t_g = 1.6\,\mu s$ (middle), both modes are driven and ϕ_0 affects the shape of the trajectories slightly; amplitude shaping is necessary to close the loops for both modes and to ensure that the net gate phase is independent of ϕ_0. Symbols correspond to steps in the pulse amplitude. For $t_g = 480\,\mathrm{ns} \approx 0.90/f_c$ (bottom), the trajectory depends strongly on ϕ_0; this simulation uses the Lamb–Dicke approximation, but the breakdown of this approximation leads to substantial gate errors because the loops no longer close.

state-preparation and readout operations. The quantum CCD architecture is a natural choice for implementing surface-code error-correction methods[17], although such methods can also be mapped onto one-dimensional ion chains. Errors due to ambient heating of the motion of the ions are proportional to t_g and will therefore be suppressed for fast gates; this is advantageous for microfabricated traps in which the ions are confined near to electrode surfaces and hence subject to greater electric field noise[25]. Spin-dephasing errors due to, for example, magnetic-field fluctuations (which typically have a $1/f$ noise spectrum), will likewise be reduced, allowing the use of qubit states that have first-order sensitivity to the magnetic field[26] (at least during gate operations, as is the case here).

The 'speed limit' set by the trap frequency f_c is not a fundamental barrier: the Coulomb interaction that is responsible for coupling the ions is almost instantaneous at the typical separation distance of trapped ions (3.5 μm here), and there have been various theoretical proposals for fast gates, with t_g less than about $1/f_c$ (see, for example, refs 8–12). None of these proposals has so far been realized, although a demonstration of the method proposed in ref. 8 has recently been reported[27], with $t_g = 18.5\,\mu s \approx 23/f_c$. Here, after first exploring the limits of the conventional $\sigma_z \otimes \sigma_z$ gate mechanism[6] (where σ_z is the Pauli operator), we implement the scheme proposed in ref. 11, in which the single rectangular laser pulse used in the conventional adiabatic method is replaced by a pulse whose amplitude is shaped in time.

The operation of the gate relies on a qubit-state-dependent force, which originates from a spatially varying light shift. This shift is caused by a 'travelling standing wave', which is generated by the optical interference pattern of two non-copropagating laser beams with frequencies that differ by ν (Fig. 1). We focus on the case of two ions, with the force coupling to only the axial modes of motion. We discuss the behaviour in three regimes: (1) a single rectangular pulse in the adiabatic regime, (2) a single rectangular pulse in the non-adiabatic regime and (3) a fast, shaped pulse or pulses.

In the first regime, by choosing $\nu = f_c + \delta$ with $\delta \ll f_c$, only the centre-of-mass normal mode at frequency f_c is excited (to a first approximation) and the rotating-wave approximation holds for the treatment of the motion. Starting from a state cooled to the Lamb–Dicke regime ($\eta^2 n \ll 1$, where η is the Lamb–Dicke parameter and n is the motional quantum number), the motion traces out an approximately circular path in the (rotating-frame) phase space of the harmonic oscillator, returning to its starting point after time $t_g = 1/\delta$ (Fig. 2). The geometric gate phase Φ is determined by the (signed) area enclosed by this path, which is proportional to Ω^2, where Ω is the Rabi frequency. We require $\Phi = \pi/2$ to generate the maximally entangled state $(|\downarrow\downarrow\rangle + i|\downarrow\uparrow\rangle + i|\uparrow\downarrow\rangle + |\uparrow\uparrow\rangle)/2$ from the separable state $(|\downarrow\downarrow\rangle + |\downarrow\uparrow\rangle + |\uparrow\downarrow\rangle + |\uparrow\uparrow\rangle)/2$ after time t_g. The gate phase Φ is independent of both the initial motional state (within the Lamb–Dicke regime) and the phase ϕ_0 of the optical beat note at the start time $t = 0$. The latter is crucial for achieving high gate fidelity in the laboratory, because ϕ_0 is sensitive to nanometre-scale length differences between the two laser-beam paths. Such gates have been implemented previously[3,6].

In the second regime, the gate time is reduced by increasing δ, but for δ comparable to f_c there are three complicating factors. First, both the centre-of-mass mode and the stretch mode (at frequency $f_s = \sqrt{3} f_c$) of a two-ion crystal will be excited and the associated trajectories in

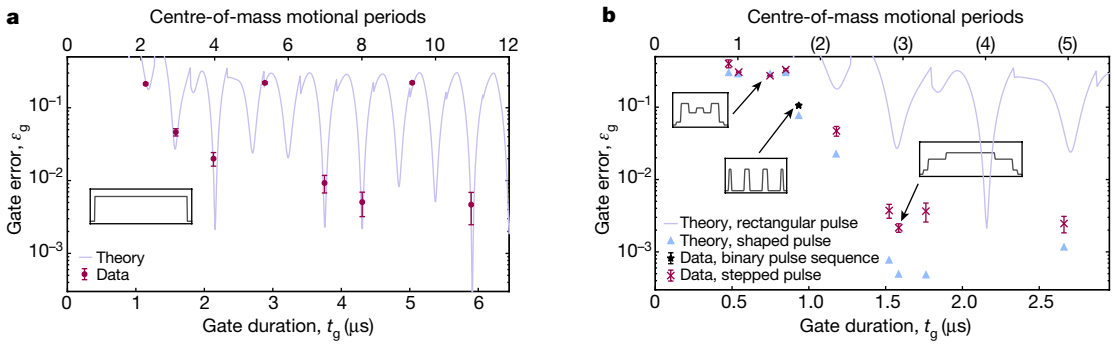

Figure 3 | Theoretical and experimental two-qubit gate errors. **a**, Conventional single, rectangular pulse (see inset). The curve shows the coherent error that is achievable (that is, excluding photon scattering and technical errors). At each time, Ω and ν are adjusted to minimize ε_g; discontinuities occur where the optimum value of ν switches between satisfying $f_c < \nu < f_s$ and $\nu > f_s$. Although a substantial reduction in gate error can be achieved by shaping the pulse edges[3] when $t_g \gg 1/f_c$, negligible improvement is possible when the gate duration becomes comparable to the shaping time constant, for $t_g \lesssim 4.5/f_c$. Data points show experimentally measured gate errors. **b**, Amplitude-shaped pulses. The values on the top axis given in parentheses are approximate. The curve from **a** is repeated for comparison (solid line). Simulated errors (triangles) are dominated by effects due to the breakdown of the Lamb–Dicke approximation for $t_g < 1.5\,\mu s$. The other points (stars, binary pulses; crosses, stepped pulses) are gate errors measured after optimizing the pulse-shape parameters using real-time feedback from the experiment. Insets illustrate example pulse shapes. Error bars in **a** and **b** show 1σ statistical errors.

phase space will not in general close at the same time. Second, the trajectories depend on ϕ_0. Third, there is a time-dependent light shift that is independent of the motion but which also depends on ϕ_0 and can result in a large single-qubit phase ϕ_{LS}. Consequently, the expected gate error has a complicated dependence on gate time, and rises steeply as the gate time approaches the period of the motion. This behaviour is demonstrated in Fig. 3a, together with a selection of results from our experiments. We measure a gate error of $\varepsilon_g = 2.0(5)\%$ for $t_g = 2.13\,\mu s$, and the theory shows that no solutions exist with lower errors at shorter times.

In the third regime, replacing the single rectangular pulse of the conventional method by a shaped pulse results in more degrees of freedom (the parameters that describe the shape of the pulse), which can be used to find especially well-performing or 'magic' pulses. In particular, we want to achieve all of the following: that the phase-space trajectories for both modes close simultaneously at $t = t_g$; that the sum of the enclosed (signed) areas is independent of ϕ_0, even though the trajectories themselves may depend on ϕ_0; that the light-shift-induced phase ϕ_{LS} is independent of ϕ_0 and preferably small; that the pulse area is small to minimize photon scattering[28]; and that the gate error is not too sensitive to errors in the parameter settings. A shaped pulse or pulse sequence is deemed a solution when it has all of these properties, and the gate error predicted for a perfectly realized sequence is below an upper bound ε_t set by practical considerations. In other words, we set ε_t well below the error that we are prepared to accept in the laboratory and search for solutions numerically.

Several classes of solution are given in ref. 11 for simple pulse shapes. We implement two types of time-symmetric sequence: a binary pulse sequence (in which a constant-amplitude force is switched on and off), and a five- or seven-segment stepped pulse. Example phase-space trajectories are shown in Fig. 2; we obtained gates up to an order of magnitude faster than those demonstrated previously. However, to understand the experimentally observed gate error and the optimal pulse shapes, we had to develop the theory further.

The solutions given in ref. 11 assume that the motion remains within the Lamb–Dicke regime. For t_g comparable to $1/f_c$ this is a poor approximation because large excursions in phase space are required to enclose sufficient area. The ions then become sensitive to the spatial variation in the force, leading to modification of the trajectories and squeezing of the motional wave packets[29]. We extend the theory by using numerical modelling to include the effects of this motional excursion beyond the Lamb–Dicke regime, and find solutions that give the minimum gate error for times in the range $200\,ns < t_g < 5.0\,\mu s$ (see Methods). The most efficient solutions, which involve optimal use of the available laser power, are found for $f_c < \nu < f_s$, when both modes are excited such that the geometric phases from each mode add constructively ($\Phi = \Phi_c + \Phi_s$). Conversely, when $\nu > f_s$, the phases subtract and more laser power is required to achieve $\Phi = \pi/2$, which in turn leads to higher photon scattering error[28]. The numerically calculated errors for some of these efficient solutions are shown in Fig. 3b, together with experimentally achieved gate errors for gate times between 480 ns and 2.7 μs (see Methods for experimental details). The fastest gate time is slightly below the centre-of-mass motional period ($1/f_c = 540\,ns$), but the error is large (40%). The binary pulse sequence achieves 11% error at $t_g = 0.93\,\mu s$. The minimum error of 0.22(3)% at $t_g = 1.6\,\mu s$ is obtained using a stepped pulse and is close to the lowest two-qubit gate errors reported previously[3,4], while the gate is 20–60 times faster. This error is an order of magnitude lower than that achievable using the conventional single-rectangular-pulse method at the same t_g. For the 1.6-μs gate, we estimate the total error due to known sources to be approximately 0.18% (Table 1).

In our set-up, the gate speed and fidelity are limited by the breakdown of the Lamb–Dicke approximation for $t_g \lesssim 1/f_c$. Faster and higher-fidelity gates are possible by reducing the Lamb–Dicke parameters (here $\eta_c = 0.126$ and $\eta_s = 0.096$); for example, decreasing the 90° angle between the two laser beams (Fig. 1b) to give $\eta_c = 0.08$ would reduce the error contribution due to the breakdown of the Lamb–Dicke approximation to 7×10^{-5}. Maintaining the same gate speed would then require higher laser intensities at the ions; although we use a moderately high laser power (about 150 mW per beam for the fastest gate), the intensity is modest (about $0.1\,mW\,\mu m^{-2}$) and the spot size ($w_0 \approx 35\,\mu m$) could be reduced substantially. Alternatively, if the optical phase ϕ_0 could be controlled sufficiently, solutions could be found for fixed ϕ_0 that allow faster gates and higher fidelities[12].

Table 1 | Error budget for the highest-fidelity and fastest gates achieved

Error source	$t_g = 1.6\,\mu s$	$t_g = 480$ ns
Lamb–Dicke-approximation breakdown	5×10^{-4}	3×10^{-1}
Optical phase chirp	$\approx 4 \times 10^{-4}$	$\approx 6 \times 10^{-3}$
Pulse timing and amplitudes	$\approx 2 \times 10^{-4}$	$\approx 1 \times 10^{-3}$
Radial mode excitation	$\lesssim 4 \times 10^{-5}$	$\lesssim 4 \times 10^{-3}$
Photon scattering	6×10^{-4}	7×10^{-3}
Centre-of-mass heating rate	8×10^{-5}	3×10^{-5}
Total error	1.8×10^{-3}	3.3×10^{-1}

The total error is the linear sum of the individual errors, on the assumption that they are constant and add incoherently.

We have demonstrated a method for realizing fast (1.6-μs duration) and robust two-qubit gates for trapped-ion qubits that combines state-of-the-art gate fidelity (99.8%) with more than an order of magnitude increase in gate speed compared to other methods. At the fastest speed demonstrated (480 ns), the fidelity achieved (60%) may not be useful for information processing, but might have other applications (such as quantum logic spectroscopy of short-lived exotic species[30,31], although this would require the use of fast laser-cooling techniques[32]). The method is technically simple, requiring only a single amplitude-shaped pulse from a continuous-wave laser, and the laser intensities required are within reach of miniature solid-state violet diodes[33]. These considerations are important if the techniques are ultimately to be scaled to the very large numbers of qubits necessary for an error-corrected quantum computer.

Online Content Methods, along with any additional Extended Data display items and Source Data, are available in the online version of the paper; references unique to these sections appear only in the online paper.

Received 4 October 2017; accepted 9 January 2018.

1. Wineland, D. J. *et al.* Experimental issues in coherent quantum-state manipulation of trapped atomic ions. *J. Res. Natl Inst. Stand. Technol.* **103,** 259–328 (1998).
2. Harty, T. P. *et al.* High-fidelity preparation, gates, memory, and readout of a trapped-ion quantum bit. *Phys. Rev. Lett.* **113,** 220501 (2014).
3. Ballance, C. J. *et al.* High-fidelity quantum logic gates using trapped-ion hyperfine qubits. *Phys. Rev. Lett.* **117,** 060504 (2016).
4. Gaebler, J. P. *et al.* High-fidelity universal gate set for $^{9}Be^{+}$ ion qubits. *Phys. Rev. Lett.* **117,** 060505 (2016).
5. Turchette, Q. A. *et al.* Deterministic entanglement of two trapped ions. *Phys. Rev. Lett.* **81,** 3631–3634 (1998).
6. Leibfried, D. *et al.* Experimental demonstration of a robust, high-fidelity geometric two ion-qubit phase gate. *Nature* **422,** 412–415 (2003).
7. Benhelm, J. *et al.* Towards fault-tolerant quantum computing with trapped ions. *Nat. Phys.* **4,** 463–466 (2008).
8. García-Ripoll, J. J., Zoller, P. & Cirac, J. I. Speed optimized two-qubit gates with laser coherent control techniques for ion trap quantum computing. *Phys. Rev. Lett.* **91,** 157901 (2003).
9. Duan, L.-M. Scaling ion trap quantum computation through fast quantum gates. *Phys. Rev. Lett.* **93,** 100502 (2004).
10. García-Ripoll, J. J., Zoller, P. & Cirac, J. I. Coherent control of trapped ions using off-resonant lasers. *Phys. Rev. A* **71,** 062309 (2005).
11. Steane, A. M. *et al.* Pulsed force sequences for fast phase-insensitive quantum gates in trapped ions. *New J. Phys.* **16,** 053049 (2014).
12. Palmero, M. *et al.* Fast phase gates with trapped ions. *Phys. Rev. A* **95,** 022328 (2017).
13. Wang, Y. *et al.* Single-qubit quantum memory exceeding ten-minute coherence time. *Nat. Photon.* **11,** 646–650 (2017).
14. Moehring, D. L. *et al.* Entanglement of single-atom quantum bits at a distance. *Nature* **449,** 68–71 (2007).
15. Barends, R. *et al.* Superconducting quantum circuits at the surface code threshold for fault tolerance. *Nature* **508,** 500–503 (2014).
16. Veldhorst, M. *et al.* A two-qubit logic gate in silicon. *Nature* **526,** 410–414 (2015).
17. Fowler, A. G. *et al.* Surface codes: towards practical large-scale quantum computation. *Phys. Rev. A* **86,** 032324 (2012).
18. Monroe, C. & Kim, J. Scaling the ion trap quantum processor. *Science* **339,** 1164–1169 (2013).
19. Devoret, M. H. & Schoelkopf, R. J. Superconducting circuits for quantum information: an outlook. *Science* **339,** 1169–1174 (2013).
20. Lin, Y. *et al.* Sympathetic electromagnetically-induced-transparency laser cooling of motional modes in an ion chain. *Phys. Rev. Lett.* **110,** 153002 (2013).
21. Bowler, R. *et al.* Coherent diabatic ion transport and separation in a multizone trap array. *Phys. Rev. Lett.* **109,** 080502 (2012).
22. Ruster, T. *et al.* Experimental realization of fast ion separation in segmented Paul traps. *Phys. Rev. A* **90,** 033410 (2014).
23. Noek, R. *et al.* High speed, high fidelity detection of an atomic hyperfine qubit. *Opt. Lett.* **38,** 4735–4738 (2013).
24. Kielpinski, D., Monroe, C. & Wineland, D. J. Architecture for a large-scale ion-trap quantum computer. *Nature* **417,** 709–711 (2002).
25. Turchette, Q. A. *et al.* Heating of trapped ions from the quantum ground state. *Phys. Rev. A* **61,** 063418 (2000).
26. Ruster, T. *et al.* A long-lived Zeeman trapped-ion qubit. *Appl. Phys. B* **122,** 254 (2016).
27. Wong-Campos, J. D., Moses, S. A., Johnson, K. G. & Monroe, C. Demonstration of two-atom entanglement with ultrafast optical pulses. *Phys. Rev. Lett.* **119,** 230501 (2017).
28. Ozeri, R. *et al.* Errors in trapped-ion quantum gates due to spontaneous photon scattering. *Phys. Rev. A* **75,** 042329 (2007).
29. McDonnell, M. J. *et al.* Long-lived mesoscopic entanglement outside the Lamb-Dicke regime. *Phys. Rev. Lett.* **98,** 063603 (2007).
30. Schmidt, P. O. *et al.* Spectroscopy using quantum logic. *Science* **309,** 749–752 (2005).
31. Meyer, V. *et al.* Measurement of the 1*s*–2*s* energy interval in muonium. *Phys. Rev. Lett.* **84,** 1136–1139 (2000).
32. Machnes, S. *et al.* Superfast laser cooling. *Phys. Rev. Lett.* **104,** 183001 (2010).
33. Schäfer, V. M. *et al.* Optical injection and spectral filtering of high-power ultraviolet laser diodes. *Opt. Lett.* **40,** 4265–4268 (2015).

Acknowledgements This work was supported by the UK EPSRC 'Networked Quantum Information Technologies' Hub, and the UK Defence, Science and Technology Laboratory. V.M.S. acknowledges funding from Balliol College, Oxford. C.J.B. acknowledges funding from Magdalen College, Oxford. We thank S. R. Woodrow for work on the trap design, T. P. Harty for contributions to the apparatus and W. Zhang for the loan of the AWG. We acknowledge the use of the University of Oxford Advanced Research Computing facility (https://doi.org/10.5281/zenodo.22558). The experiments benefitted from the use of the ARTIQ control system (https://doi.org/10.5281/zenodo.591804).

Author Contributions C.J.B. performed the numerical modelling. V.M.S. and C.J.B. designed and performed the experiments and analysed the data. K.T. built the ion trap and characterized the fast AOMs. L.J.S. and T.G.B. built optical and control systems. V.M.S., C.J.B., A.M.S. and D.M.L. wrote the manuscript, which all authors discussed.

Author Information Reprints and permissions information is available at www.nature.com/reprints. The authors declare no competing financial interests. Readers are welcome to comment on the online version of the paper. Publisher's note: Springer Nature remains neutral with regard to jurisdictional claims in published maps and institutional affiliations. Correspondence and requests for materials should be addressed to D.M.L. (d.lucas@physics.ox.ac.uk).

METHODS

Numerical modelling. Most trapped-ion experiments can be described in the Lamb–Dicke regime, in which the optical field is assumed to be uniform over the extent of the wavefunction of each ion. However, for the large phase-space displacements necessary to perform fast gates, this assumption breaks down—the curvature of the field can no longer be neglected. This means that the force experienced by an ion depends on its displacement in phase space, and this leads to squeezing of the wavefunction and modification of the motional trajectory.

To model the coherent error of a given gate sequence, we therefore numerically integrate the full Hamiltonian (without making the Lamb–Dicke approximation) using the split-operator method, explicitly averaging over different initial optical phases. Because this is a computationally intensive process, the gate sequences used in the experiments were preselected by an efficient solver that works in the Lamb–Dicke regime. Following ref. 11, we optimize candidate solutions starting from a random seed, and select a set of candidate solutions that have an error of less than 10^{-4} in the Lamb–Dicke approximation.

These candidate solutions were then evaluated using the full solver, and the most promising were optimized further. For the experiments, we chose solutions from this set by looking for a combination of low coherent error and low integrated pulse area (this both selects for a low photon scattering error[28] and avoids fragile sequences that use large motional excitations, which are more sensitive to parameter variations).

We evaluated several different pulse shapes. The seven-segment symmetric pulse shape offered a sufficient number of parameters to find a dense set of good solutions, while being easy to implement and to verify. The exact shape of the rising and falling edges is unimportant: the rise time can be varied from zero to the segment length without a change in gate fidelity, providing that an overall scaling factor is applied to the Rabi frequency of the gate to compensate for the changing spectral content.

Raman beams. The light source for the Raman beams is a frequency-doubled Ti:sapphire laser (M-Squared SolsTiS ECD-X) with 1.8-W output power at 397 nm. The Raman detuning was $\Delta = -1$ THz for single rectangular pulses; for shaped-pulse gates with $t_g \leq 1\,\mu$s, $\Delta = -200$ GHz; and for $t_g > 1\,\mu$s, $\Delta = -800$ GHz. The detuning was changed to reduce photon scattering errors for gates that require lower Rabi frequencies. For the fastest gate, peak powers of 192 mW and 96 mW were used for the two Raman beams, which had waists at the ions of 33 μm and 38 μm, respectively ($1/e^2$ intensity radius). The ratios of the Raman-beam intensities were chosen so that the scattering error was approximately minimized. The beams were modulated by a pair of acousto-optic modulators (AOMs; Brimrose CQM-200-40-.400/OW), with a 24-ns rise time (10%–90%) to create the shaped pulses that drive the gate. The amplitude-shaped radio-frequency (200-MHz) signal for the stepped pulse was defined using an arbitrary-waveform generator (AWG; Agilent N8241A, 1.25-GHz clock rate, 15 bits vertical resolution) and fed to the first AOM. The second AOM was driven by a direct digital synthesis (DDS; Enterpoint Milldown card, 200 MHz) source (Fig. 1b).

Phase chirps of the modulated beam were measured in an optical homodyne experiment and found to be substantial during switching of the radio-frequency amplitude. Driving the AOM at its centre frequency (200 MHz) minimized the phase chirps[34] so that their contribution to the gate error was small (Table 1).

Pulse calibration. Performing fast gates with high fidelities requires precise control of the pulse parameters. Owing to the nonlinear response of the AOM for different radio-frequency drive amplitudes, the pulse shape was measured on a photodiode and the relative drive amplitudes of each pulse segment were adjusted to match the measured amplitudes to their theoretically predicted optimum levels. The relative amplitudes of the stepped pulses were set with ±0.2% accuracy. Although the exact shape of the rising and falling edges is not critical, for a given shape the duration of the pulse segments needs to be set with subnanosecond precision. The waveform programmed into the 1.25 Gsps (1 Gsps = 10^9 samples per second) AWG had a 5.0-ns rise time, to spread the pulse edges over several time points and to improve the effective timing resolution. The timing precision of the optical pulses was measured to be 0.2 ns (standard deviation of fitted pulse lengths). Setting the pulse-shape parameters to their theoretically predicted values yielded optimal fidelity for all gate sequences for which the Lamb–Dicke approximation held well. There are three remaining parameters that characterize the gate sequence: the peak beam power, the Raman beat-note frequency ν and the phase offset $\phi_{\pi/2}$ of the last $\pi/2$ pulse of the Ramsey interferometer ($\phi_{\pi/2}$ compensates for the single-qubit phase that is acquired during the gate). The beat-note frequency and beam power were set to their theoretically predicted values and then optimized empirically; in all cases the optimized values agreed well with the theoretical predictions. The peak pulse powers of each beam were stabilized at the beginning of each experimental sequence. The phase offset $\phi_{\pi/2}$ was calibrated empirically. Initially gate parameters were optimized using a Nelder–Mead algorithm, using real-time feedback from the experiment. After the minimization of the optical phase chirps, this optimization method was no longer necessary and linear optimization of single parameters was found to be sufficient. A list of parameters for the fastest and highest-fidelity gates is given in Extended Data Table 1.

Experimental procedure. All gates were performed in a blade-type linear Paul trap[35,36], with axial centre-of-mass frequency $f_c = 1.92$ MHz for $t_g > 1\,\mu$s, and $f_c = 1.86$ MHz for $t_g \leq 1\,\mu$s and for all single-rectangular-pulse gates. The axial frequency was changed after re-aligning the Raman beams to suppress coupling to radial modes. In both cases the axial frequency was chosen so that the ion spacing was $12.5\lambda_z$, where $\lambda_z = 283$ nm is the periodicity of the travelling standing wave that provides the gate force. The gate was performed on the qubit states $|\downarrow\rangle = 4S_{1/2}|F=4, M=+4\rangle$ and $|\uparrow\rangle = 4S_{1/2}|F=3, M=+3\rangle$ in $^{43}Ca^+$ at $B = 14.6$ mT. (This value of the B-field gives access to the 'atomic clock' qubit states $|\downarrow'\rangle = 4S_{1/2}|F=4, M=0\rangle$ and $|\uparrow'\rangle = 4S_{1/2}|F=3, M=+1\rangle$ with long coherence time T_2^*, measured previously[2] to be roughly 1 min, which are ideal for use as a memory qubit.) The ions were laser-cooled using dark-resonance Doppler cooling[37] to $\bar{n} \approx 1.8$ and further cooled using sideband cooling to $\bar{n} \lesssim 0.05$. After state preparation in $|\downarrow\downarrow\rangle$, we created an entangled state by placing the geometric phase gate in one arm of a Ramsey interferometer split by a spin-echo π pulse[6]. The gate errors were determined by using partial tomography[38] to measure the fidelity of the created state with respect to the desired state $(|\downarrow\downarrow\rangle + |\uparrow\uparrow\rangle)/\sqrt{2}$.

Error analysis. All gate errors and fidelities quoted are after correction for state-preparation and readout errors[3]. The total state-preparation and readout error with two ions was typically $\bar{\varepsilon}_{\mathrm{SPAM}} = 1.4(1) \times 10^{-3}$ per ion (averaged over both qubit states). The 0.22(3)% error reported for the $t_g = 1.6\,\mu$s gate is the average of five experimental runs measured over two days. Directly after calibrating the experimental parameters, the lowest error measured was 0.15(3)%; an hour after calibration, the measured error was 0.28(3)%. Quoted uncertainties are statistical only. We also measured the accumulated error for concatenated sequences of up to seven gates and found no evidence of coherent errors.

Errors due to radial-mode excitation are largest for gate times of $t_g \approx 800$ ns, because in this case the Raman beat-note frequency ν is close to resonance with the radial-mode frequencies (about 4.2 MHz). With the final alignment of the Raman laser beam we can limit errors due to radial-mode excitation to $\varepsilon_g < 5 \times 10^{-2}$ at $t_g = 800$ ns. An advantage of fast gates is that they are insensitive to errors associated with motional decoherence or heating: despite the relatively large heating rate of this trap ($\dot{\bar{n}} \approx 100\ \mathrm{s}^{-1}$ for the axial centre-of-mass mode), the contribution to the gate error is negligible. A summary of the main errors present in our experiments, for the lowest-error gate and for the fastest gate, is given in Table 1.

Data availability. The data shown in Figs 1–3 and that support the other findings of this study are available from the corresponding author on reasonable request.

34. Degenhardt, C. *et al.* Influence of chirped excitation pulses in an optical clock with ultracold calcium atoms. *IEEE Trans. Instrum. Meas.* **54,** 771–775 (2005).
35. Gulde, S. T. *Experimental Realization of Quantum Gates and the Deutsch–Josza Algorithm with Trapped $^{40}Ca^+$-Ions.* PhD thesis, Univ. Innsbruck (2003).
36. Woodrow, S. R. *Linear Paul Trap Design for High-fidelity, Scalable Quantum Information Processing.* MSc thesis, Univ. Oxford (2015).
37. Allcock, D. T. C. *et al.* Dark-resonance Doppler cooling and high fluorescence in trapped Ca-43 ions at intermediate magnetic field. *New J. Phys.* **18,** 023043 (2016).
38. Sackett, C. A. *et al.* Experimental entanglement of four particles. *Nature* **404,** 256–259 (2000).

Extended Data Table 1 | Gate parameters used for the fastest gate (seven segments) and for the highest-fidelity gate (five segments)

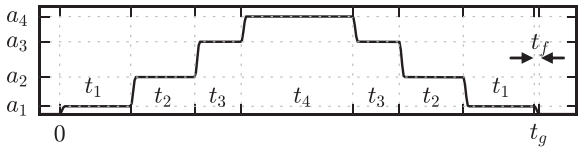

parameter	gate duration $t_g = 483\,\text{ns}$	gate duration $t_g = 1.59\,\mu\text{s}$
Raman detuning Δ	$-200\,\text{GHz}$	$-800\,\text{GHz}$
Raman beat note frequency ν	$6.3802\,\text{MHz}$	$2.6301\,\text{MHz}$
axial centre-of-mass frequency f_c	$1.8615\,\text{MHz}$	$1.9243\,\text{MHz}$
peak power (pulse-shaped beam)	$192\,\text{mW}$	$58\,\text{mW}$
power (non-shaped beam)	$96\,\text{mW}$	$48\,\text{mW}$
single-qubit phase $\phi_{\pi/2}$	$91.4°$	$21.4°$
pulse time t_1	$71.4\,\text{ns}$	$82.1\,\text{ns}$
pulse time t_2	$64.5\,\text{ns}$	$299.9\,\text{ns}$
pulse time t_3	$46.7\,\text{ns}$	—
pulse time t_4	$112.3\,\text{ns}$	$819.5\,\text{ns}$
pulse fall-time t_f	$5.0\,\text{ns}$	$5.0\,\text{ns}$
pulse amplitude a_1	0.284	0.445
pulse amplitude a_2	0.617	0.838
pulse amplitude a_3	0.862	—
pulse amplitude a_4	1	1

The pulse envelope (top) illustrates the definition of the pulse amplitude and timing parameters ($t_g = 2t_1 + 2t_2 + 2t_3 + t_4 + t_f$). The timing parameters refer to the timing of the waveform programmed into the AWG, for which a $t_f = 5.0$ ns rise/fall time (0%–100%) was used; the measured rise/fall time (10%–90%) of the laser pulses was 24 ns, owing to the bandwidth of the particular AOMs used (see Fig. 2a). The waists ($1/e^2$ intensity radii) of the Raman beams were 33 μm and 38 μm for the pulse-shaped and non-shaped beams, respectively.